

# Precise radiochromic film dosimetry using a flat-bed document scanner

Slobodan Devic,<sup>a)</sup> Jan Seuntjens, Edwin Sham, and Ervin B. Podgorsak  
*Medical Physics Department, McGill University Health Centre, Montréal, Québec H3G 1A4, Canada*

C. Ross Schmidlein and Assen S. Kirov  
*Memorial Sloan-Kettering Cancer Center, New York, New York*

Christopher G. Soares  
*Ionizing Radiation Division, National Institute of Standards and Technology, Gaithersburg, Maryland 20899*

(Received 8 December 2004; revised 19 April 2005; accepted for publication 20 April 2005; published 15 June 2005)

In this study, a measurement protocol is presented that improves the precision of dose measurements using a flat-bed document scanner in conjunction with two new GafChromic® film models, HS and Prototype A EBT exposed to 6 MV photon beams. We established two sources of uncertainties in dose measurements, governed by measurement and calibration curve fit parameters contributions. We have quantitatively assessed the influence of different steps in the protocol on the overall dose measurement uncertainty. Applying the protocol described in this paper on the Agfa Arcus II flat-bed document scanner, the overall one-sigma dose measurement uncertainty for an uniform field amounts to 2% or less for doses above around 0.4 Gy in the case of the EBT (Prototype A), and for doses above 5 Gy in the case of the HS model GafChromic® film using a region of interest  $2 \times 2 \text{ mm}^2$  in size. © 2005 American Association of Physicists in Medicine. [DOI: 10.1118/1.1929253]

Key words: radiochromic film dosimetry, flat-bed scanner, uncertainty analysis, sensitivity curves

## I. INTRODUCTION

Their high spatial resolution, minor energy dependence, and near tissue-equivalence make radiochromic films (RCF)<sup>1,2</sup> appropriate for dose distribution measurements in megavoltage radiation fields with high dose gradients. Radiochromic media were initially developed for dose measurements in industrial radiation processing.<sup>3-6</sup> Having only a  $6 \mu\text{m}$  thick sensitive layer, these relatively insensitive films were suitable for dose measurements between 50 and 2500 Gy (model HD-810 or DM-1260, Nuclear Associates). (In this paper, certain commercially available products are referred to by name. These references are for informational purposes only and do not imply that these are the best or only products available for the purpose, and do not imply endorsement by the National Institute of Standards and Technology.) A more sensitive model, the MD-55-1 (Nuclear Associates),<sup>7,8</sup> was developed that had a  $15 \mu\text{m}$  thick sensitive layer and covered a dose range from 10 to 100 Gy. Subsequently, a more sensitive model, the MD-55-2, was introduced that was composed of two MD-55-1 layers (separated by a central inert binding layer).<sup>9-12</sup> Currently, the MD-55-2 model is available commercially under the name MD-55 GafChromic® film and it covers a dose range from 1 to 250 Gy.

Several types of instruments (single-point densitometers, and one- or two-dimensional position-sensitive light detector densitometers) are used for two-dimensional film dosimetry.<sup>13-15</sup> Although not specifically designed for radiochromic film dosimetry, document scanners have previously been used for measurements in various film dosimetry applications.<sup>16,17</sup> Flat-bed document scanners designed for

high quality photographic scanning with an option to operate in transmission mode usually employ a fluorescent light source with a broadband emission spectrum and a linear charge coupled device (CCD) array detector. These scanners allow the acquisition of transmission scans in up to a 48-bit red-green-blue (RGB) mode, e.g., 16 bits per color. Since the absorption spectrum of the radiochromic film exhibits a maximum in the red region of the visible spectrum, as previously determined by Stevens *et al.*,<sup>16</sup> extraction of the red channel from the RGB image can improve document scanner sensitivity when used in combination with radiochromic films. The idea of using the red channel of the RGB transmission image for radiochromic film dosimetry has been subsequently employed by many authors.<sup>14,17-22</sup>

Amongst the various scanning densitometers used for the radiochromic film dosimetry tasks, many of these utilize lasers as a light source, providing coherent and polarized light. However, these two properties of laser light can lead to serious problems when using laser-based optical densitometers for radiochromic film dosimetry. Dempsey *et al.*<sup>23</sup> have demonstrated that laser light coherence can create interference patterns, and made recommendations on methods for their removal. In addition, radiochromic films have been shown to have a relatively small variation in optical density when the light source is linearly polarized and the film is rotated.<sup>24,25</sup> However, if the light source and the detector are both linearly polarized, variations in the measured optical density can amount to 15% for the HS model GafChromic® film<sup>25</sup> when the film is rotated through  $360^\circ$ . Corrections can be made for these two effects, but the flat-bed document scanners that

employ a noncoherent broadband (white) light emission spectrum do not require these corrections, and are thus inherently simpler and more reliable for precise optical density measurements.

Dose measurements based on any film dosimetry system have uncertainties inherent to the particular system used. By using a uniform radiation field during the process of calibration, the overall combined absorbed dose measurement uncertainty is limited to three main factors: (1) the overall uncertainty of the dose measurement in the reference field; (2) the uncertainty due to the nonuniform thickness of the film's sensitive layer; and (3) uncertainties associated with the densitometer used to measure optical density (for a classification of uncertainties, see Ref. 26) of the irradiated film sample.

Although the sensitivity of the MD-55 film model is relatively high, its dose response range is limited to relatively high doses in comparison to everyday clinical practice. Recently, two new radiochromic film models, HS (high sensitivity) and EBT (external beam therapy) have been introduced. The EBT model has two sensitive layers, whereas the HS model has a single sensitive layer, and both models were designed for two-dimensional dose measurements in high-energy photon beams (above 1 MeV).

Every film dosimetry system consists of three main components: the film model used, the scanning densitometer, and the scanning protocol. In this study we establish a protocol that provides a high dose measurement precision while using a flat-bed document scanner in combination with two new GafChromi® film models, the HS and Prototype A EBT.

## II. MATERIALS AND METHODS

### A. Radiochromic films

The HS GafChromic® film model (International Specialty Products, Wayne, NJ) has been developed as a more sensitive and uniform alternative to the GafChromic® MD-55 film. It was specifically designed for the measurement of absorbed dose in high-energy photon and electron beams (above 1 MeV). According to the manufacturer, the HS model covers a dose range from 1 to 50 Gy. Film consists of a single active layer sandwiched between two sheets of clear, transparent polyester [Fig. 1(a)], each with thickness of approximately  $97\ \mu\text{m}$  and density of  $1.35\ \text{g}/\text{cm}^3$ . The HS active layer has a thickness of  $40\ \mu\text{m}$  and nominally consists of H (9%), C (57%), N (16%), and O (18%) by weight as quoted by the manufacturer.

The EBT model high-sensitivity radiochromic film has been tailored for absorbed dose measurements in high-energy photon beams employed in intensity-modulated radiation therapy (IMRT). As quoted by the manufacturer, the film is designed to be used in a dose range from 0.01 to 8 Gy. The structure of the new EBT film (Prototype A) model is more complex than that of the HS model, and consists of two sensitive layers, each having thickness of  $17\ \mu\text{m}$  and separated by a  $6\ \mu\text{m}$  thick surface layer [Fig. 1(b)], all sandwiched between two  $0.97\ \mu\text{m}$  clear polyester sheets. The overall atomic composition of the EBT GafChromic film

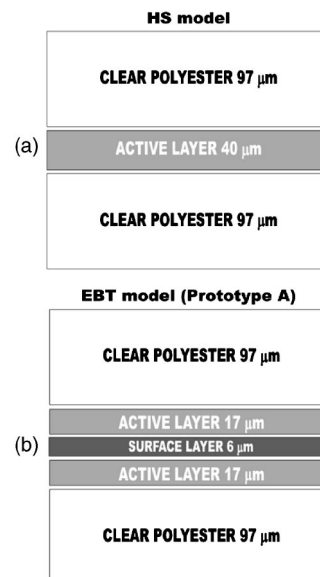


FIG. 1. Diagram of the GafChromic® film structure/dimensions: (a) HS model and (b) EBT model-Prototype A.

model is H (39.7%), C (42.3%), O (16.2%), N (1.1%), Li (0.3%), and Cl (0.3%) as quoted by the manufacturer.

Figure 2 shows the absorption spectra for the two new radiochromic film models. In order to measure the absorption spectra of the film samples, an HP 8452A Diode-Array Spectrophotometer was used. The pieces of film were placed in the standard sample compartment. A special plastic adapter was fabricated to ensure that the surface of the film was perpendicular to the direction of the light beam. The acquisitions were taken after a 4-h warm-up time and each spectrum was measured with an exposure time of 1 s.

All radiochromic film models have similar absorption spectra with a maximum absorption band centered at 678 nm, while the absorption spectrum of the new EBT model exhibits a similar shape but is shifted toward shorter wavelengths. The maximum absorption band for the EBT model is centered at 633 nm, the wavelength that corresponds to the emission of the He-Ne laser. However, serious polarization effects have been observed with this new radiochromic film model (N. Klassen and C. Ross, private communication), and one has to be extremely careful when using a He-Ne laser-based densitometer. It is apparent from Fig. 2 that the EBT model is about ten times more sensitive than the HS model, if the optical density change is measured with a monochromatic light source centered at the corresponding absorption maxima, 633 nm for the EBT film model and 678 nm for the HS film model.

The film's batch numbers used in this work were L0445HS for the HS film and 34194-03 for the EBT film (Prototype A). At the time of this study, the EBT GafChromic® film model was still under clinical and technical evaluation.

### B. Phantom and irradiation procedures

Samples of film were placed at the isocenter of the accelerator, in a source-axis distance (SAD) setup at a distance of

100 cm. A  $20 \times 20$  cm<sup>2</sup> field size at the isocenter was used. The films were covered with a 10 cm thick piece of solid water and a 15 cm thick piece of solid water was placed below the films, to provide sufficient backscatter. At 10 cm downstream from this bottom piece, an additional ionization chamber was placed to monitor the linac output during the irradiation process and to determine the dose delivered to the film.

For both film models, we prepared five film packets. Each packet consisted of ten pieces of the HS GafChromic® film or ten pieces of the EBT film. The HS GafChromic® films were exposed to the following doses: 0, 1.0, 2.5, 4.9, 7.7, 10.0, 20.4, 30.6, 40.7, and 50.1 Gy at McGill University. The EBT films were exposed at Memorial Sloan-Kettering Cancer Center (MSKCC) to the following doses: 0, 0.1, 0.3, 0.5, 0.7, 3.1, 5.1, 7.2, 11.3, and 15.4 Gy. The film samples were handled in accordance with recommendations outlined in the AAPM TG-55 report.<sup>1</sup> The film pieces were only removed from their light-protecting envelope during irradiation and readout to reduce the effects of ambient light.<sup>27</sup> For both film models, four film packets have been used for the calibration procedure. The fifth (“test”) film packet for both film models was used to test the validity of the radiochromic film dosimetry protocol described in this paper.

Film samples ( $2.5 \times 1.5$  cm<sup>2</sup> in size) were irradiated with a 6 MV photon beam from a Varian 21 EX accelerator (Varian, Palo Alto, CA). The films were exposed perpendicularly to the radiation beam in a  $30 \times 30 \times 25$  cm<sup>3</sup> solid water RMI-457 phantom. The region of interest (ROI) analyzed was a 2 mm by 2 mm square in the middle of the upper half of the film piece, positioned 5 mm from the upper film edge, to avoid optical density (OD) measurement artifacts that have been observed near film edges.<sup>27</sup> The bottom half of the film was used for labeling and handling.

### C. Scanning procedure

In this study, we used an Agfa Arcus II desktop flat-bed document scanner, whose technical characteristics are described elsewhere.<sup>1,14</sup> Film pieces are scanned using the Agfa FotoLook 3.5 software, with the maximum OD range and all filters and image enhancement options turned off. Once the scanner is turned on, it is important to perform a preview operation in transmission mode and then allow the scanner to warm-up for half an hour. This operation turns on the upper lamp used for transmission mode and allows its temperature to stabilize. By default the scanner only turns on the bottom (reflective) lamp, which causes the signal from the transmission measurements to gradually decrease in time, due to transmission light warm-up. Also, we kept the transparency module raised so that the warming of the transmission lamp does not increase the temperature of the transparent glass plate. The films were scanned in the 48-bit RGB mode (16 bits per color) and saved as tagged image file format (TIFF) image files.

The first step in the protocol is to scan the unexposed pieces of film five times. Multiple scans have been performed in order to remove the scanner noise by subsequent

averaging of the scanned images. Once the five images of the unexposed film pieces have been acquired, blank scans are taken (again five times) over the same scanning region as the previously acquired images with the film pieces. This allows one to correct for “defective” pixels, defined as pixels that differ in intensity from the blank (unattenuated) signal, which is equal to  $2^{16}$ .

The film packets were then irradiated in accordance with the procedure described in Sec. II B. Once irradiated, the films were left for a period of 48 h to self-develop, and then they were scanned again five times with the same orientation as the un-irradiated scans. This allowed film-to-film co-registration, and avoidance of image rotation, which can introduce unnecessary averaging of adjacent pixels. In general, scanned images with irradiated films will have a scanning region different from that of the un-irradiated film pieces. Therefore, for the removal of the defective pixels in irradiated film images, five blank scans are made again of the irradiated film scanning region.

Five successive scans were chosen for the scanning protocol because preliminary studies showed that averaging of more than five scans does not significantly improve signal measurement reproducibility. In fact, a preliminary study showed that due to the summing in quadrature of a constant random noise, averaging more than five images results in a slight increase of the relative uncertainty signal over a given region of interest. After averaging over five scans, the relative standard deviation over a given ROI reaches a minimum of 0.16% and then increases to 0.2% if ten successive scans are averaged.

All images were scanned with an image resolution of 0.113 mm/pixel. Accordingly,  $2 \times 2$  mm<sup>2</sup> ROIs in which the net optical densities (*netOD*) were determined consisted of 18 by 18 pixels.

### D. Image processing

The scanning procedure thus results in four sets of images: unexposed films, irradiated films, and two sets of blank (no film) scans obtained after each of them. Once four sets of five images were obtained, the images were imported into an in-house image manipulation routine written with MatLab 6.5.0 (Math Works, Natick, MA) that extracts the red component of the RGB scanned image and subsequently determines the *netOD* of the irradiated film pieces.

The first step in the processing of the images was the identification of defective pixels. Since two glass plates are in the optical pathway (in addition to the examined film) the system can exhibit many imperfections. These can be recognized as deviation from the theoretical value of  $2^{16}$  for certain points within the scanning region of the empty bed caused by specks or dust on the light pathway from the lamp to the CCD detector. This identification was performed over the resulting images obtained by averaging five successive scans of the empty bed, for both un-irradiated and irradiated film images. We found that the percentage of faulty pixels was smaller than 0.4% ( $3.68 \times 10^{-3}$ ).

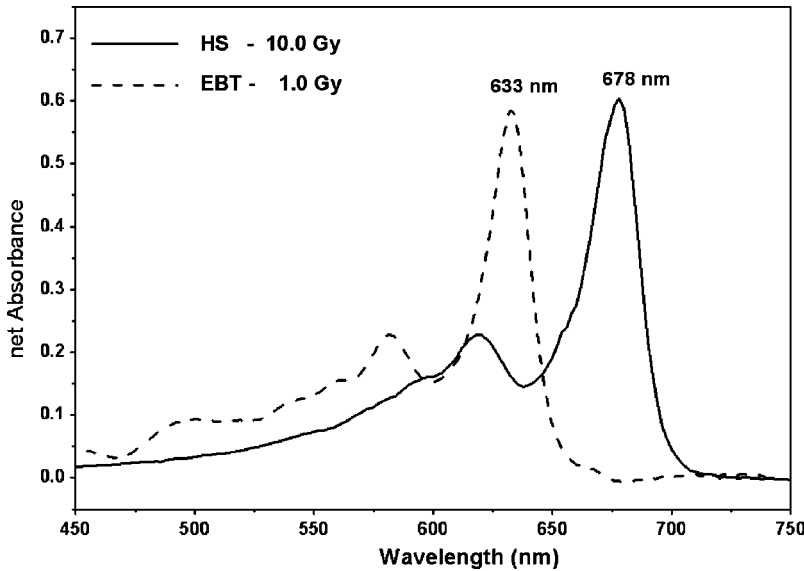


FIG. 2. The net optical absorption spectra measured with an HP 8452A Diode-Array Spectrophotometer for the two GafChromic® film models, exposed to different doses of 6 MV photon beams: the EBT film model (Prototype A) was irradiated to 1 Gy, whereas the HS film model was irradiated to a dose of 10 Gy.

Once the faulty pixels had been identified, the film images were first averaged, a 2D zero-phase Wiener filter was applied to the averaged images, and the points recognized as defective were discarded. Averaging of multiple successive scans was done with the intention of removing the noise caused by the scanner, whereas the application of the adaptive Wiener filter (in  $7 \times 7$  pixel regions)<sup>28</sup> was meant to decrease the image noise caused by the imperfections in the film sample. The 2D Wiener filter, which uses a local estimate of the noise power spectrum, was applied since it preserves systematic variations in the film’s optical density. The transmission scanner readings ( $I_{unexp}$  or  $I_{exp}$ ) as well as the standard deviations ( $\sigma_{I_{unexp}}$  or  $\sigma_{I_{exp}}$ ) were determined for every film piece as a mean pixel value over the ROI.

The zero-light transmitted intensity value ( $I_{bckg}$ ), which characterizes the background signal of the scanner, as well as its corresponding standard deviation ( $\sigma_{bckg}$ ), were determined over the same ROI with an opaque piece of film. Opaque pieces of film were simulated by using stacks of three  $1.5 \times 2$  cm<sup>2</sup> pieces of XV-2 radiographic film which had been removed from their protecting envelope, left on a light box for half an hour, and then subsequently developed. To simulate the actual scanning conditions, ten opaque film

sets were placed in a single row, along the CCD collimation direction. Finally, values for  $I_{bckg}$  and  $\sigma_{bckg}$  were determined as weighted averages over the ten simulated opaque film pieces.

**E. Dose response relation**

In this section we present calculation of the *netOD* based on our previous work<sup>14</sup> for the case where multiple film packets have been used for the calibration procedure.

For densitometers that do not read *OD* directly, the  $netOD^i(D_j)$  and the  $\sigma_{netOD}^j(D_j)$  for a dose  $D_j$  can be calculated as follows:

$$\begin{aligned}
 netOD^i(D_j) &= OD_{exp}^i(D_j) - OD_{unexp}^i(D_j) \\
 &= \log_{10} \frac{I_{unexp}^i(D_j) - I_{bckg}}{I_{exp}^i(D_j) - I_{bckg}}, \tag{1}
 \end{aligned}$$

where  $I_{unexp}^i(D_j)$  and  $I_{exp}^i(D_j)$  are the readings for unexposed and exposed film piece for the *i*th film packet, respectively, while  $I_{bckg}$  is the zero-light transmitted intensity value, and using an error propagation expression that ignores cross correlations,<sup>26</sup>

$$\sigma_{netOD}^j(D_j) = \frac{1}{\ln 10} \sqrt{\frac{(\sigma_{I_{unexp}}^j(D_j))^2 + (\sigma_{bckg})^2}{(I_{unexp}^j(D_j) - I_{bckg})^2} + \frac{(\sigma_{I_{exp}}^j(D_j))^2 + (\sigma_{bckg})^2}{(I_{exp}^j(D_j) - I_{bckg})^2}}. \tag{2}$$

All quantities in Eqs. (1) and (2) are calculated over the same ROI for every film piece in each film packet. The final *netOD* for a particular dose point ( $D_j$ ) was determined as a weighted mean:

$$netOD(D_j) = \frac{\sum_{i=1}^N (netOD^i(D_j) / (\sigma_{netOD}^j(D_j))^2)}{\sum_{i=1}^N (1 / (\sigma_{netOD}^j(D_j))^2)}, \tag{3}$$

where the corresponding uncertainties were calculated as

$$(\sigma_{netOD}(D_j))^2 = \frac{1}{\sum_{i=1}^N (1/(\sigma_{netOD}^i(D_j))^2)}, \quad (4)$$

and the summation is over the  $N$  calibration packets of film samples. Delivered dose ( $D$ ) versus measured  $netOD$  was fitted using the analytical form

$$D_{fit} = b \cdot netOD + c \cdot netOD^n \quad (5)$$

following the approach outlined in our previous work.<sup>14</sup>

## F. Dose uncertainty analysis

In a previous paper<sup>14</sup> an uncertainty analysis for radiochromic film dose measurements was presented that separates an experimental contribution from the uncertainty contribution due to the calibration curve fit. In this section, we summarize the results of this dose uncertainty analysis.

The relative experimental uncertainty of the measured dose for the established functional form given by Eq. (5) is given by

$$\sigma_{D_{exp}}(\%) = \frac{\sqrt{(b + n \cdot c \cdot netOD^{n-1})^2 \cdot \sigma_{netOD}^2}}{D_{fit}} \times 100, \quad (6)$$

with  $\sigma_{netOD}$  calculated using Eq. (4), whereas the relative fit uncertainty is expressed as

$$\sigma_{D_{fit}}(\%) = \frac{\sqrt{netOD^2 \cdot \sigma_b^2 + netOD^{2 \cdot n} \cdot \sigma_c^2}}{D_{fit}} \times 100, \quad (7)$$

where  $\sigma_b$  and  $\sigma_c$  represent the fitting parameter uncertainties.

Finally, the total relative uncertainty for the dose measured using the above described formalism for the functional form given by Eq. (5) is calculated as

$$\sigma_{D_{tot}}(\%) = \frac{\sqrt{netOD^2 \cdot \sigma_b^2 + netOD^{2 \cdot n} \cdot \sigma_c^2 + (b + n \cdot c \cdot netOD^{n-1})^2 \cdot \sigma_{netOD}^2}}{D_{fit}} \times 100. \quad (8)$$

## III. RESULTS

### A. Dose response curves

The calibration curves for the two film models under investigation are shown in Fig. 3. The points correspond to the measured values of  $netOD$  change with dose for each type of film determined using Eq. (3). In the same graph, the corresponding error bars of one standard deviation around the mean, calculated using Eq. (4), are drawn, but are not visible because they are smaller than the symbols in the figure. Fit curves shown in Fig. 3 are given by Eq. (5). For both types of film, the fit procedures returned the best results for a fitting parameter  $n=2.5$ . The parameters  $b$  and  $c$  (together with their corresponding uncertainties) are also included in the graph.

Figure 3 indicates that at the  $netOD$  level of 1 the sensitivity of the EBT film model is three times higher than that for the HS film model, both determined with the AGFA scanner. This value is significantly lower than stated in Sec. II A as the  $netOD$  is not measured at the maximum of the absorption peak (Fig. 2), but instead represents an average over the red part of the light source emission spectrum. When using the broadband emission light source, even if only the red component is extracted, a different sensitivity is obtained when compared to the monochromatic absorption measurements.

### B. Dose uncertainty estimates

Establishing uncertainties in measured doses is particularly important in clinical applications where high dose gradients (as in the case of IMRT fields) are commonly present.

In addition, in most experimental measurement applications, once the system has been calibrated, only a single measurement with a single film piece will be taken. Typically, in order to estimate the uncertainties on these types of measurements only single data values will be available to relate the  $netOD$  measurements to the unknown doses. Therefore, the remaining test film packet from each batch, which was not used for the calibration fit procedure, was used to estimate uncertainties on unknown doses measured using the above described protocol. From now on, we will consider that the film pieces in the remaining test film packets were exposed to “unknown” doses.

Using the expression given by Eq. (5) we have calculated the “unknown” doses for each piece of film in both of the test film packets. Also, by using Eq. (9) we calculated the total uncertainties for each film piece in both test film packets. Figure 4 summarizes components of the dose uncertainty for the AGFA Arcus II system with the film models under investigation. It shows that the fit uncertainty, calculated using Eq. (8), is approximately constant while the experimental uncertainty, calculated using Eq. (7), drops with increasing dose. From the insets in Fig. 4, the conclusion can be drawn that application of the protocol described in this work can result in a measurement dose uncertainty of 2% using the AGFA Arcus II flat-bed scanner for doses above 0.4 Gy for the EBT film and for doses above 5 Gy with the HS GafChromic® film.

In order to assess the influence of different steps of the proposed dosimetry protocol, a step-by-step analysis for the EBT film model has been performed. The results of this analysis are summarized in Fig. 5.

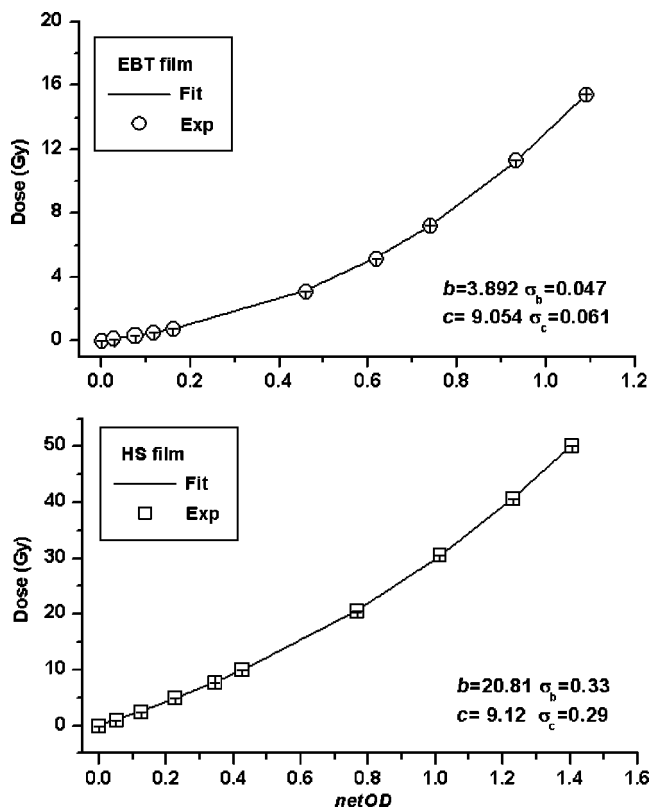


FIG. 3. Calibration curves for two GafChromic® film models and AGFA Arcus II flat-bed document scanner: above—EBT (Prototype A), below—HS.

The upper-left portion of Fig. 5 represents the results of the uncertainty analysis using only one film packet for the calibration. In this approach only a single scan was performed without any additional image analysis. As a result, an overall uncertainty  $<5\%$  was observed with the EBT film in combination with the Agfa Arcus II scanner for doses above 2 Gy.

However, if a single film packet is used for calibration, but with the film images scanned five times and then averaged (Fig. 5, upper right), the overall uncertainty improves, providing a level of uncertainty of less than 3% for doses above 2 Gy. As expected for this case, the experimental uncertainty, given by Eq. (7), decreases, while the fit uncertainty, given by Eq. (8), remains the same.

In the next step, four different calibration packets were introduced (Fig. 5, bottom left). This resulted in a further reduction of the fit uncertainty, from 4% to 3% for the first dose point at 0.1 Gy. Finally, the introduction of the defective pixel correction and a 2D, zero-phase Wiener filter provided the best uncertainty estimates in this analysis, i.e., less than 2% for doses above 0.4 Gy.

For the HS GafChromic® film, an improvement of dose uncertainty from 3% for doses above 10 Gy to 2% for doses above 5 Gy was achieved.

### C. Justification of the uncertainty analysis

In order to justify the uncertainty analysis, described in Sec. II F with Eq. (9), a regression analysis of the functional

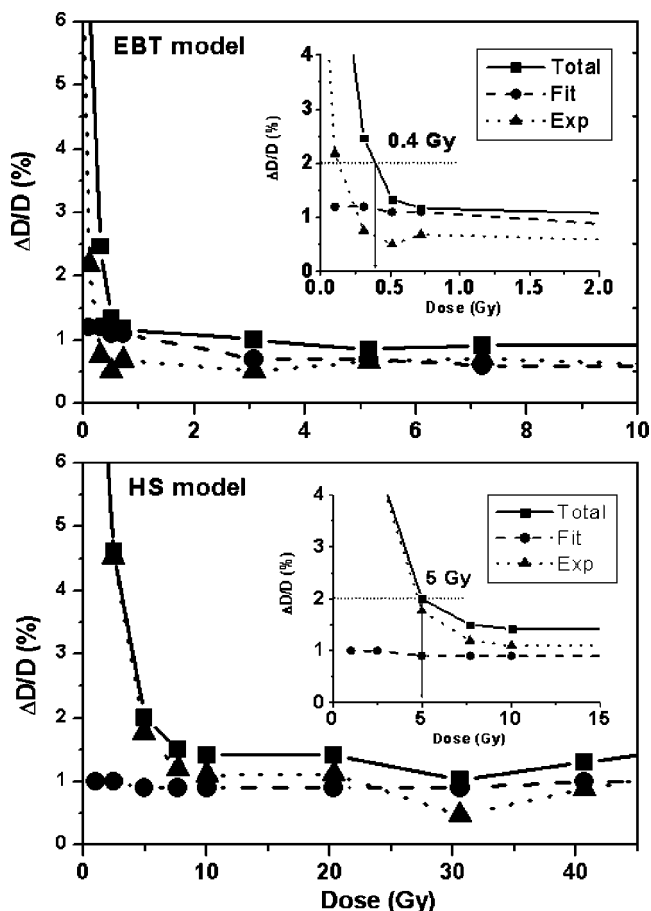


FIG. 4. Uncertainty estimates for a single test film set measurement for two film types: above—EBT (Prototype A), below—HS. Squares—total relative dose uncertainty [Eq. (8)], circles—fit relative dose uncertainty [Eq. (7)], and triangles—experimental relative dose uncertainty [Eq. (6)].

dependence of the dose determined for film pieces exposed to “unknown” doses using Eq. (5) (calculated dose) and the dose to the film as determined with the downstream ionization chamber (delivered dose) was performed. The linear fit was carried out by using the inverse square of total uncertainties, calculated with Eq. (9) for each dose point, as weighting factors for a particular test film packet. Moreover, points that correspond to doses smaller than 0.4 Gy in the case of the EBT film and doses smaller than 5 Gy in the case of the HS film model have been discarded from the linear fit procedure because of low signal levels. The slope,  $a$ , of the fitted line differs from unity for the HS model GafChromic® film by less than 1% and is within the one-sigma fit uncertainty, i.e.,  $a=0.994\pm 0.010$ , whereas for the EBT film model, the regression analysis gives  $a=0.996\pm 0.009$ .

In Figs. 6(a) and 6(b), we present the error between the delivered dose and the calculated dose for the HS film model and the EBT film model, respectively. The two figures confirm the results of our uncertainty analysis that 2% one-sigma uncertainty for the HS film model can be achieved for doses above 5 Gy, and for doses above 0.4 Gy for the EBT (Prototype A) GafChromic® film model. This type of graph can be used as a verification tool for future application of

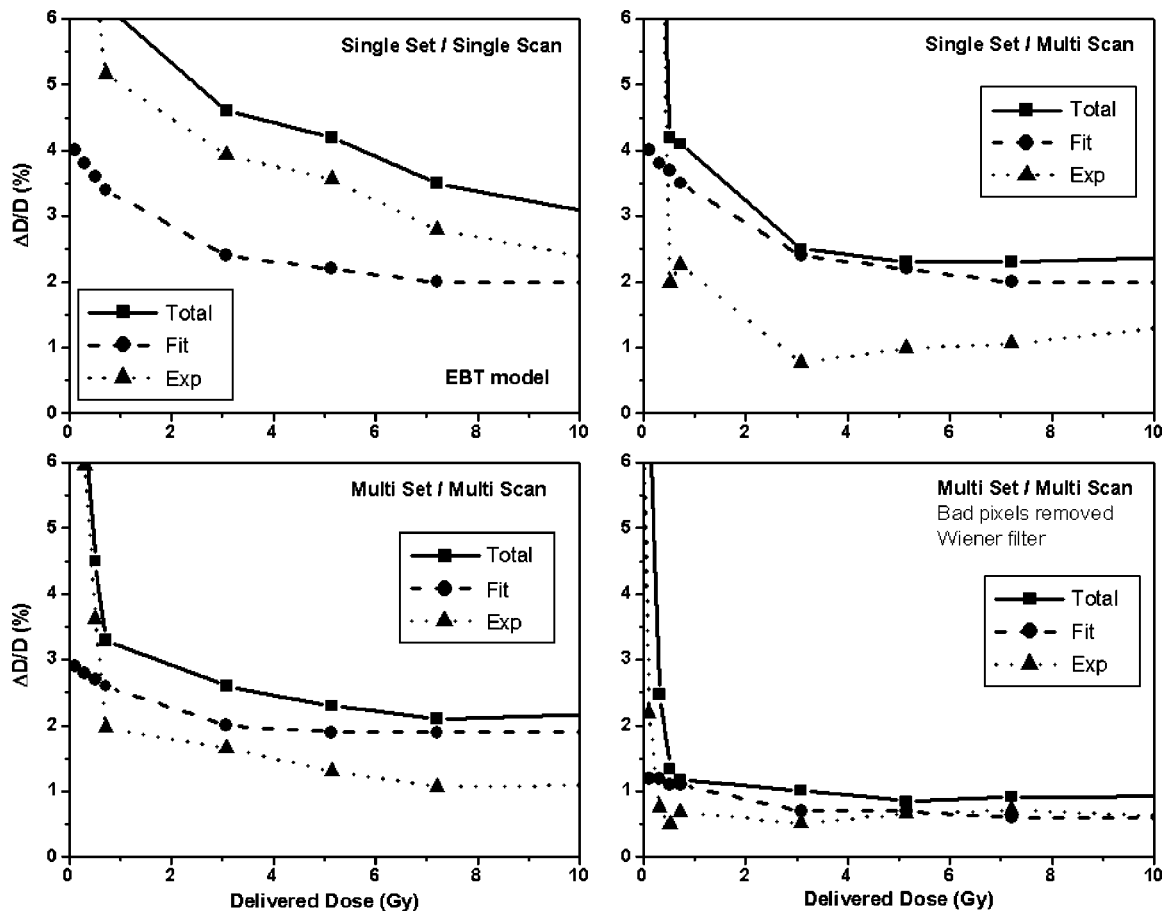


FIG. 5. Influence of different image analysis and uncertainty analysis procedures on the overall dose uncertainty, as well as on two of its components (fit and experimental) for EBT (Prototype A) GafChromic® film model.

once established calibration curve. The properties of radiochromic films may change with changes of environmental conditions, length of the post-irradiation waiting period, and batch number. Plotting the graph described in Fig. 6 can be used as a verification that, for a deemed uncertainty limits, the protocol and the corresponding calibration curve are still valid.

#### D. Protocol summary

The radiochromic film dosimetry protocol described in this paper can be summarized in two steps (Fig. 7). The first step (the calibration step) involves determination of the functional form given by Eq. (5) for a given radiochromic film model and particular flat-bed document scanner. The second step corresponds to the measurement of an unknown 2D dose distribution, as well as uncertainty estimates of the dose determined using this protocol.

To calibrate the radiochromic film dosimetry system the following actions are recommended:

- (i) Multiple film packets, containing film pieces of  $\sim 1.5$  cm by  $\sim 2.5$  cm in size, are prepared with the number of pieces in each packet covering a dose range intended for future applications; one film packet

(“test” packet) should be reserved for the calibration verification through a plot such as on Fig. 6.

- (ii) Unexposed pieces of film are scanned multiple (we recommend five) times in a transmission mode using, preferably a 48-bit RGB color contone scanning mode with all the image enhancement filters turned off; five blank scans of the scanner bed are performed over the same scanning region, as for the unexposed film pieces, for defective pixel identification.
- (iii) The film pieces are exposed to a series of known doses; the use of a monitor chamber, positioned well below the plane in which the films are positioned, is recommended to verify the dose delivered to the film.
- (iv) A time delay is introduced to allow the radiochromic film to self-develop, at least 6 h for EBT film and 24 hours for the HS film model.
- (v) After the film self-development waiting period, the film pieces are placed onto the scanner bed and multiple (five) images are acquired with the same scanning parameters as in item (ii) above; then another five blank scans of the scanner bed are performed over the same scanning region, as that of the exposed film pieces, for defective pixel identification. At this

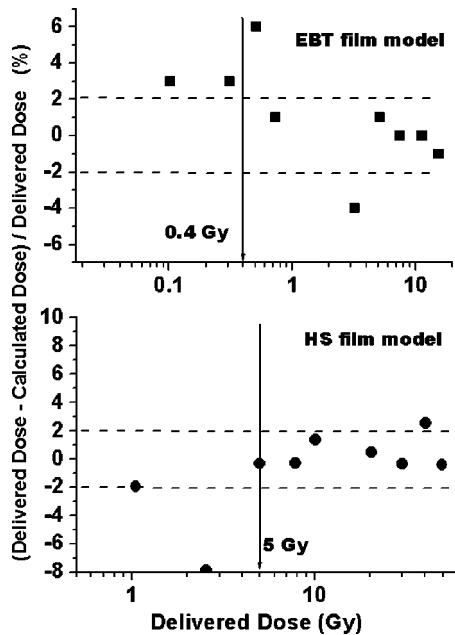


FIG. 6. Justification of the uncertainty estimation analysis: relative percent error in dose calculated using Eq. (5) with respect to dose delivered to the particular test film packet as a function of delivered dose for EBT (above) and HS (below) GafChromic film model.

point, measurement of the zero-light transmission intensity value ( $I_{bckg}$ ), measured with an opaque piece of film, is recommended.

- (vi) Blank images at the unexposed and exposed film positions are averaged and the faulty pixels are identified; within the average unexposed and exposed film images, the “bad” pixels are discarded or replaced by the average values of the neighboring pixels; a 2D Wiener filter is then applied to both resultant images, and the transmission scanner readings ( $I_{unexp}$  or  $I_{exp}$ ) as well as the standard deviations ( $\sigma_{I_{unexp}}$  or  $\sigma_{I_{exp}}$ ) are determined for every film piece as a mean pixel value over the desired ROI.
- (vii) For every film packet, the  $netOD^i$  [Eq. (1)] and the corresponding  $\sigma_{netOD}^i$  [Eq. (2)] are calculated and  $netOD$  and  $\sigma_{netOD}$  are determined using Eqs. (3) and (4). In such a way, calculated  $netOD$  values are plotted as a function of delivered dose and then fitted with the functional form given by Eq. (5) in order to determine the power  $n$  as well as the fit parameters  $b$  and  $c$  and their corresponding fitting uncertainties.
- (viii) Dose uncertainty assessment, based on Fig. 4, as well as verification of the calibration curve and dose uncertainty analysis, based on Fig. 6, should be performed by using the “test” film packet.

The following actions are recommended during the unknown dose measurement process:

- (i) The unexposed piece of film is scanned multiple (five) times in the transmission mode using the same scanning parameters as in the case of the calibration procedure; five blank scans of the scanner bed are per-

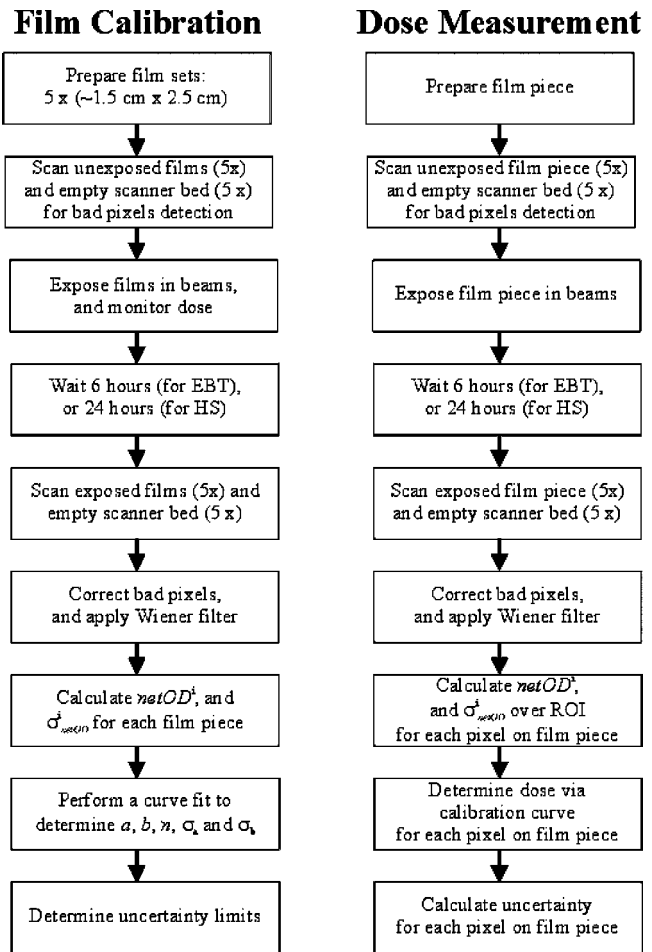


FIG. 7. Summary of the radiochromic film dosimetry protocol.

formed over the same scanning region, as with the unexposed film piece, for the sake of faulty pixel identification.

- (ii) The film piece is exposed to an unknown dose.
- (iii) The same waiting time as in the case of the calibration process is used for the radiochromic film to self-develop. Subsequently, the film piece is placed on the scanner bed and multiple (five) images are acquired with the same scanning parameters as in point (i) above; after removal of the exposed film pieces another five blank scans of the scanner bed are performed over the same scanning region, as that of the exposed film piece, for defective pixel identification.
- (iv) Within averaged unexposed and exposed images, bad pixels are discarded or replaced by the average values of the neighboring pixels; the 2D Wiener filter is applied to both unexposed and exposed film resultant images.
- (v) Resulting unexposed and exposed images are co-registered and resized to the pixel size being equal to the ROI size used during the calibration procedure, resulting in four new images:  $I_{unexp}(i, j)$ ,  $\sigma_{unexp}(i, j)$ ,  $I_{exp}(i, j)$ , and  $\sigma_{exp}(i, j)$ . The  $netOD(i, j)$  given in Eq.

(1) and the corresponding  $\sigma_{netOD}(i,j)$  given in Eq. (2) are calculated for every pixel  $(i,j)$  within the resulting image. Using Eq. (5), the calculated *netOD* values are converted to an 2D dose image of unknown doses, while the corresponding total relative uncertainties can be calculated using Eq. (8) resulting in 2D dose uncertainty image.

#### IV. CONCLUSIONS

In this study a radiochromic dosimetry protocol is established for use with radiochromic film exposed to 6 MV photon beams and read with a flat-bed document scanner. Two sources of uncertainty, which are characteristic of the radiochromic film dosimetry process, are considered. These are the experimental uncertainty, and the function fitting parameters uncertainty, both determined during the calibration process. Each step in the protocol has been quantitatively assessed in order to determine their influence on the overall dose measurement uncertainty.

In the case of the EBT film, the protocol described in this work can provide a 2% dose measurement uncertainty for a uniform field with the AGFA Arcus II flat-bed scanner for doses above around 0.4 Gy, and in the case of the HS model GafChromic® film the protocol with this scanner can provide a 2% dose measurement uncertainty for doses above 5 Gy.

#### ACKNOWLEDGMENTS

We would like to thank Dr. David Lewis from ISP for useful discussions. J. S. is a research scientist of the National Cancer Institute Canada appointed with funds provided by the Canadian Cancer Society.

<sup>a)</sup> Author to whom correspondence should be addressed. Electronic mail: devic@medphys.mcgill.ca

<sup>1</sup>A. Niroomand-Rad, C. R. Blackwell, B. M. Coursey, K. P. Gall, J. M. Galvin, W. L. McLaughlin, A. S. Meigooni, R. Nath, J. E. Rodgers, and C. G. Soares, "Radiochromic film dosimetry: Recommendations of AAPM Radiation Therapy Committee Task Group 55," *Med. Phys.* **25**, 2093–2115 (1998).

<sup>2</sup>M. J. Butson, K. N. Yu, T. Cheung, and P. E. Metcalfe, "Radiochromic film for Medical Radiation Dosimetry," *Mater. Sci. Eng., R.* **41**, 61–120 (2003).

<sup>3</sup>W. L. McLaughlin, J. C. Humphreys, D. Hocken, and W. J. Chappas, "Radiochromic dosimetry for validation and commissioning of industrial radiation processes," in *Progress in Radiation Processing*, Proceedings of the Sixth International Meeting, Ottawa, 1987, edited by F. M. Fraser [*Radiat. Phys. Chem.* **31**, 505–514 (1988)].

<sup>4</sup>M. C. Saylor, T. T. Tamargo, W. L. McLaughlin, H. M. Khan, D. F. Lewis, and R. D. Schenfele, "A thin film recording medium for use in food irradiation," *Radiat. Phys. Chem.* **31**, 529–536 (1988).

<sup>5</sup>R. D. H. Chu, G. Van Dyke, D. F. Lewis, K. P. J. O'Hara, B. R. Buckland, and F. Dinelle, "Gaf-chromic dosimetry media: A new high dose rate thin film routine dosimeter and dose mapping tool," *Radiat. Phys. Chem.* **35**, 767–773 (1990).

<sup>6</sup>W. L. McLaughlin, Y. D. Chen, C. G. Soares, A. Miller, G. Van Dyke, and D. F. Lewis, "Sensitometry of the response of a new radiochromic film dosimeter to gamma radiation and electron beams," *Nucl. Instrum. Methods Phys. Res. A* **302**, 165–176 (1991).

<sup>7</sup>M. J. Butson, J. N. Mathur, and P. E. Metcalfe, "Radiochromic film as a

radiotherapy surface-dose detector," *Phys. Med. Biol.* **41**, 1073–1078 (1996).

<sup>8</sup>W. L. McLaughlin, J. M. Puhl, M. Al-Sheikhly, C. A. Christou, A. Miller, A. Kovacs, L. Wojnarovits, and D. F. Lewis, "Novel radiochromic films for clinical dosimetry," *Radiat. Prot. Dosim.* **66**, 263–268 (1996).

<sup>9</sup>T. D. Bohm, D. W. Pearson, and R. K. Das, "Measurements and Monte Carlo calculations to determine the absolute detector response of radiochromic film for brachytherapy dosimetry," *Med. Phys.* **28**, 142–146 (2001).

<sup>10</sup>G. Menon and R. Sloboda, "Measurement of relative output for <sup>90</sup>Sr ophthalmic applicators using radiochromic film," *Med. Dosim* **25**, 171–177 (2000).

<sup>11</sup>S. Meigooni, M. F. Sanders, G. S. Ibbott, and S. R. Szeglin, "Dosimetric characteristics of an improved radiochromic film," *Med. Phys.* **23**, 1883–1888 (1996).

<sup>12</sup>Y. Zhu, A. Kirov, A. Mishra, A. Meigooni, and J. Williamson, "Quantitative evaluation of radiochromic film response for two-dimensional dosimetry," *Med. Phys.* **24**, 223–231 (1997).

<sup>13</sup>G. R. Gluckman and L. E. Reinstein, "Comparison of three high-resolution digitizers for radiochromic film dosimetry," *Med. Phys.* **29**, 1839–1846 (2002).

<sup>14</sup>S. Devic, J. Seuntjens, G. Hegyi, E. B. Podgorsak, C. G. Soares, A. S. Kirov, I. Ali, J. F. Williamson, and A. Elizondo, "Dosimetric properties of improved GafChromic films for seven different digitizers," *Med. Phys.* **31**, 2392–2401 (2004).

<sup>15</sup>S.-T. Chiu-Tsao, T. Duckworth, C. Zhang, N. S. Patel, C.-Y. Hsiung, L. Wang, J. Allen Shih, and L. B. Harrison, "Dose response characteristics of new models of GafChromic films: Dependence on densitometer light source and radiation energy," *Med. Phys.* **31**, 2501–2508 (2004).

<sup>16</sup>M. A. Stevens, J. R. Turner, R. P. Hugtenburg, and P. H. Butler, "High-resolution dosimetry using radiochromic film and a document scanner," *Phys. Med. Biol.* **41**, 2357–2365 (1996).

<sup>17</sup>D. A. Low, J. F. Dempsey, J. Markman, S. Mutic, E. E. Klein, J. W. Sohn, and J. A. Purdy, "Toward automated quality assurance for intensity-modulated radiation therapy," *Int. J. Radiat. Oncol., Biol., Phys.* **53**, 443–452 (2002).

<sup>18</sup>M. Bazioglou and J. Kalef-Ezra, "Dosimetry with radiochromic films: a document scanner technique, neutron response, applications," *Appl. Radiat. Isot.* **55**, 339–345 (2001).

<sup>19</sup>S. Aydarous, P. J. Darley, and M. W. Charles, "A wide dynamic range, high-spatial-resolution scanning system for radiochromic dye films," *Phys. Med. Biol.* **46**, 1379–1389 (2001).

<sup>20</sup>H. Alva, H. Mercado-Urbe, M. Rodriguez-Villafuerte, and M. E. Brandan, "The use of a reflective scanner to study radiochromic film response," *Phys. Med. Biol.* **47**, 2925–2933 (2002).

<sup>21</sup>A. Mack, G. Mack, D. Weltz, S. G. Scheib, H. D. Bottcher, and V. Seifert, "High precision film dosimetry with GafChromic films for quality assurance especially when using small fields," *Med. Phys.* **30**, 2399–2409 (2003).

<sup>22</sup>G. Thomas, R. Y. Chu, and F. Rabe, "A study of GafChromic XR Type R film response with reflective-type densitometers and economical flatbed scanners," *J. Appl. Clin. Med. Phys.* **4**, 307–314 (2003).

<sup>23</sup>J. F. Dempsey, D. A. Low, A. S. Kirov, and J. F. Williamson, "Quantitative optical densitometry with scanning-laser film digitizers," *Med. Phys.* **26**, 1721–1731 (1999).

<sup>24</sup>N. Klassen, L. van der Zwan, and J. Cygler, "GafChromic MD-55: investigated as a precision dosimeter," *Med. Phys.* **24**, 1924–1934 (1997).

<sup>25</sup>M. J. Butson, P. K. N. Yu, T. Cheung, and D. Inwood, "Polarization effects on a high-sensitivity radiochromic film," *Phys. Med. Biol.* **48**, N207–N211 (2003).

<sup>26</sup>P. R. Bevington and D. K. Robinson, *Data Reduction and Error Analysis for the Physical Sciences* (WCB/McGraw-Hill, Boston, 1992).

<sup>27</sup>M. J. Butson, P. K. N. Yu, and P. E. Metcalfe, "Effects of read-out light sources and ambient light on radiochromic film," *Phys. Med. Biol.* **43**, 2407–2412 (1998).

<sup>28</sup>J. S. Lim, *Two-Dimensional Signal and Image Processing* (Prentice Hall, Englewood Cliffs, NJ, 1990).